BMC Medical Imaging

RESEARCH Open Access

A CT-based radiomics analyses for differentiating drug-resistant and drug-sensitive pulmonary tuberculosis

Fengli Jiang[1,3], Chuanjun Xu[2*], Yu Wang[1] and Qiuzhen Xu[1*]

Abstract

Background To explore the value of computed tomography based radiomics in the differential diagnosis of drug-sensitive and drug-resistant pulmonary tuberculosis.

Methods The clinical and computed tomography image data of 177 patients who were diagnosed with pulmonary tuberculosis through sputum culture and completed drug-susceptibility testing from April 2018 to December 2020 at the Second Hospital of Nanjing were retrospectively analyzed. Patients with drug-resistant pulmonary tuberculosis ($n=78$) and drug-sensitive pulmonary tuberculosis ($n=99$) were randomly divided into a training set ($n=124$) and a validation set ($n=53$) at a ratio of 7:3. Regions of interest were drawn to delineate the lesions and radiomics features were extracted from non-contrast computed tomography images. A radiomics signature based on the valuable radiomics features was constructed and a radiomics score was calculated. Demographic data, clinical symptoms, laboratory results and computed tomography imaging characteristics were evaluated to establish a clinical model. Combined with the Rad-score and clinical factors, a radiomics-clinical model nomogram was constructed.

Results Thirteen features were used to construct the radiomics signature. The radiomics signature showed good discrimination in the training set (area under the curve (AUC), 0.891; 95% confidence interval (CI), 0.832–0.951) and the validation set (AUC, 0.803; 95% CI, 0.674–0.932). In the clinical model, the AUC of the training set was 0.780(95% CI, 0.700-0.859), while the AUC of the validation set was 0.692 (95% CI, 0.546–0.839). The radiomics-clinical model showed good calibration and discrimination in the training set (AUC, 0.932;95% CI, 0.888–0.977) and the validation set (AUC, 0.841; 95% CI, 0.719–0.962).

Conclusions Simple radiomics signature is of great value in differentiating drug-sensitive and drug-resistant pulmonary tuberculosis patients. The radiomics-clinical model nomogram showed good predictive, which may help clinicians formulate precise treatments.

Keywords Pulmonary tuberculosis, Drug-resistant, Computed tomography, Radiomics, Nomogram

*Correspondence:
Chuanjun Xu
xchuanjun@163.com
Qiuzhen Xu
xuqiuzhen831@sina.com
[1]Department of Radiology, Medical School, Zhongda Hospital, Southeast University, 87 Dingjiaqiao Road, Nanjing 210009, China
[2]Department of Radiology, The Second Hospital of Nanjing, Nanjing University of Chinese Medicine, Nanjing City 210003, Jiangsu Province, China
[3]Department of Radiology, Zhejiang Cancer Hospital, Hangzhou 310022, China

Background

Tuberculosis (TB) is a chronic, granulomatous, and necrotizing disease caused by infection with *Mycobacterium tuberculosis* and is the second most lethal infectious disease [1]. Since 1997, the World Health Organization (WHO) has annually released a global tuberculosis report. The Global Tuberculosis Report 2022 released by the WHO indicated an estimated 10.6 million new-onset TB patients in the world in 2021, and the number of TB deaths globally increased from 2019 to 2021, reversing the downward trend from 2005 to 2019 [2]. In addition, the burden of drug-resistant (DR) TB increased between 2020 and 2021. In 2021, there were 450,000 new patients with rifampicin-resistant tuberculosis. Pulmonary tuberculosis can be divided into primary drug-resistant tuberculosis (initially infected with drug-resistant *Mycobacterium tuberculosis*) and acquired drug-resistant tuberculosis (due to long treatment time, poor patient compliance, abuse of anti- tuberculosis drugs, and screening for drug-resistant *Mycobacterium tuberculosis* at lower than optimal levels) by way of infection with drug-resistant *Mycobacterium tuberculosis*. The treatment of DR-TB patients requires prompt replacement of second-line anti-TB medications, which are more expensive and have longer hospitalizations and greater risk of serious adverse effects, thus posing new challenges to global TB prevention and control [3].

According to the WHO guidelines, the detection of TB and resistance requires bacteriological confirmation, and drug resistance testing using rapid molecular testing, culture methods or sequencing techniques. However, culturing *Mycobacterium tuberculosis* from clinical samples is time-consuming(more than 8 weeks), and rapid molecular detection is expensive and is difficult to carry out in remote areas [4, 5]. Moreover, resistance genes have not been fully discovered, which may lead to false negative results in the detection of some drug-resistant *Mycobacterium tuberculosis* strains. Thus, it is necessary to distinguish between drug sensitive (DS) and DR-TB in time in order to effectively manage tuberculosis patients and control the spread of *Mycobacterium tuberculosis* [6].

Previous studies suggested that the coexistence of multiple drug-resistant CT signs of pulmonary tuberculosis can provide an imaging basis for timely drug resistance detection of suspected drug-resistant pulmonary tuberculosis (DR-PTB) patients [7–9]. However, the imaging features of DR-TB and DS-TB overlap, and the application of naked eye observation is subjective and limited, which presents challenges for radiologists.

Recently, advances in radiomics have improved the processes of extracting quantitative features from medical images with the help of computer software and the selection of the most valuable radiomics features for clinical assistance based on statistics or machine learning [10]. At present, the application of radiomics in pulmonary TB is differential diagnosis with single lesion such as mass cryptococcus, and pulmonary adenocarcinoma [11, 12]. However, few studies have applied radiomics to multiple lesions. The purpose of this study was to construct a radiomics signature, a clinical model and a radiomics-clinical model to explore the value of CT-based radiomics in the differential diagnosis of DR-TB and DS-TB. The performance of radiomics-clinical model nomogram was assessed with respect to calibration, discrimination, and clinical usefulness.

Methods

Patient cohort

Our Institutional Review Board approved this retrospective study with a waiver of informed consent. We retrospectively collected the clinical and CT image data of 764 TB patients (DR-TB, $n=164$; DS-TB, $n=600$) who were diagnosed through sputum culture and have completed drug-susceptibility testing from April 2018 to December 2020 at the Second Hospital of Nanjing. The inclusion criteria were like following: [1]TB patients who were confirmed by sputum culture and have completed drug-susceptibility testing; and [2]TB patients who had abnormal chest CT images and complete clinical data. The exclusion criteria were as follows: [1] patients without chest non-contrast CT scan on admission or with inadequate quality images; and [2] patients with incomplete clinical data; [3] patients with hematogenous disseminated TB or tuberculous pleurisy; and [4] patients that complicated with lung cancer, lung interstitial diseases or other severe lung diseases or infected with AIDS or other pathogenic microorganisms. All patients were randomly divided into two cohorts at a ratio of 7:3 using FeAture Explorer (https://github.com/salan668/FAE), with 124 cases in the training dataset and 53 cases in the validation dataset [13].

Clinical data acquisition

Clinical information, including demographic data, clinical symptoms and laboratory test results, was also recorded. Baseline epidemiologic and clinical characteristics, including age, gender, diagnosis type (initial treatment or retreatment), history of diabetes, clinical symptoms of cough and sputum, hemoptysis, night sweats, fever, chest tightness and shortness of breath, fatigue and emaciation, and laboratory tests, such as C-reactive protein (CRP) and the erythrocyte sedimentation rate (ESR), were obtained from medical records. Clinical symptoms were defined as symptoms at the time of admission, and laboratory examinations were carried out by blood test within 3 days after admission. Patients at initial diagnosis were those who had not been treated with anti-tuberculosis drugs in the past or who

had not completed the course of treatment with regular drugs after starting chemotherapy. Retreatment of pulmonary TB is as follows: [1] patients who failed in initial treatment; [2] patients who were positive for sputum bacteria again after receiving regular medication; and [3] patients who received irregular chemotherapy for more than 1 month.

CT image acquisition

All patients underwent CT with a Philips Brilliance spiral 64-CT equipment. The CT scanning parameters were as follows: 120 kV, 87 mA, a slice thickness of 3 mm and an interval of 3 mm. All patients used a unified approach when scanning. The patient was in a supine position, with both hands raised above the head. They were instructed to perform breath-holding during CT acquisition, which was performed first from the chest entrance down to the base of the lung.

CT features evaluation

We selected the CT examination that was closest to the sputum culture (interval time, 30 days) for CT features evaluation. If there were multiple groups of CT image data, we selected the data that were most closely related to drug susceptibility testing. Two experienced radiologists (one resident, and the other with more than 15 years of imaging diagnosis experience), who were blinded to the clinic-pathologic data, evaluated the CT features by consensus. The following features were evaluated in the radial DICOM viewer software: number of lung lobes involved, emphysema, atelectasis, bronchial wall thickening, bronchiectasis, bronchial dissemination, pulmonary exudation, pulmonary proliferation, calcification, nodule or mass, fibrosis, cavities (number、number of lung lobes involved、with or without calcification or fluid plane, type of cavity wall), pleural effusion, pleural thickening, pleural thickening with calcification and collapsed thoracic cages. Note: pulmonary exudation included ground glass opacity and consolidation.

Construction of the clinical factor model

Univariate analysis was used to compare the differences in clinical factors (including clinical data and CT features) between the two groups. A multivariable logistic regression analysis was applied to construct the clinical factor model by using the significant variables (P<0.05) from the univariate analysis as inputs. Variables were also dropped if collinearity existed.

Three-dimensional segmentation of tuberculosis images

We used DICOM (digital imaging and communications in medicine) images of axial CT plain scan for radiomics features extraction based on the Dr. Wise Lung Analyzer scientific research platform. All images are not preprocessed or normalized. All pulmonary lesions, that is region of interest (ROI), were delineated in 3 mm thick lung window (window width, 1600HU; window center, −500HU), which is easier to show pulmonary lesions than the mediastinal window and convenient to outline ROI thus reducing the consumption of manpower and material resources. A doctor with the qualification certificate of medical practitioner manually delineated the three-dimensional ROI, and a radiologist with more than 15 years of experience reviewed and corrected the delineated ROI. The principle of delineation is to draw all pulmonary lesions that can be distinguished by naked eyes layer by layer along the outline of the lesion. An example of manual segmentation is presented in Fig. 1A-C.

Radiomics feature extraction and construction of the radiomics signature

Radiomic features extracted through Pyradiomics software 3.0 (https://pyradiomics.readthedocs.io/en/latest/) included following: first-order features, shape features, gray level co-occurrence matrix (GLCM), gray level run-length matrix, (GLRLM), gray level size zone matrix (GLSZM), neighborhood gray-tone difference matrix (NGTDM), gray level dependence matrix (GLDM).

The least absolute shrinkage and selection operator (LASSO) was performed to select the most valuable features from the training set. We used the five-fold cross validation method to screen the super parameters γ in

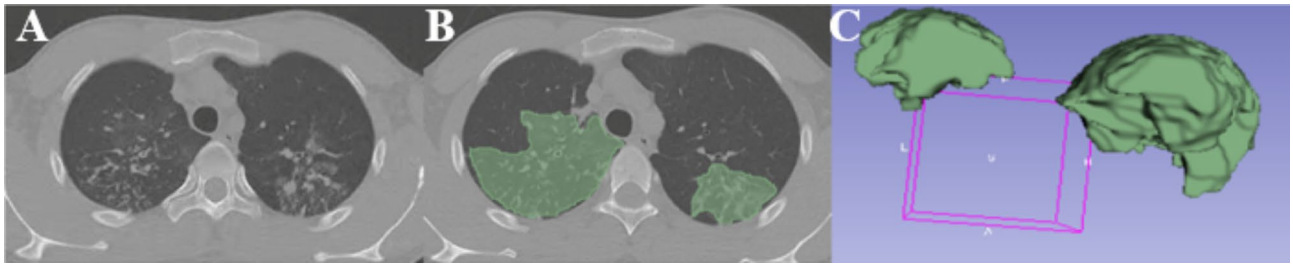

Fig. 1 Manual three-dimensional segmentation of the TB lesions. (**A**). Lesions on the axial slice; (**B**). Segmentation on the axial slice; (**C**). Three-dimensional volumetric reconstruction

the LASSO regression model. The selected features were applied to construct a radiomics signature. Radiomics scores (Rad-score) was calculated for each patient through a linear combination of the extracted features with their respective coefficients.

Construction of a combined model with clinical candidate factors and rad-score

Multivariable backward logistic regression analysis was adopted to establish a comprehensive radiomics-clinical model by combination of rad-score and clinical candidate factors. The results of the comprehensive model are represented by the radiomics-clinical model nomogram for visualization.

Assessment of the performance of difference models

The diagnostic performance of the clinical factor model, the radiomics signature and the radiomics-clinical model nomogram for differentiating DR-PTB from DS-PTB was evaluated based on the area under the curve (AUC) of the receiver operating characteristic curve (ROC), sensitivity, specificity, and accuracy in both the training and validation sets. The prediction model validation of nomogram was performed using bootstrapping with 1000 resamples to plot the calibration curve to analyze the calibration of the nomogram. Decision curve analysis (DCA) was performed to assess the clinical usefulness of the nomogram.

Statistical analysis

Statistical analyses were performed by using SPSS 20.0 and R software (version 4.1.1). The quantitative data conforming to the normal distribution was expressed by means±standard deviation, and the contrast between groups was evaluated by t test. If the data did not conform to a normal distribution, the Mann–Whitney U-test was used to indicate the median and quartile [M(P25,P75)]. Count data was expressed by rate and comparison was performed by chi-square test. Multivariate and univariate logistic regression analysis was used to compare the value of each rad-score, and clinical factors for the differentiation of DR-TB from DS-TB. The "glmnet" package was used to perform LASSO regression model analysis. The "pROC" package was used to plot the ROC curves. The "RMS" package was used to plot the nomogram and calibration curves. The "dca.R" package was applied to plot the decision curve. A two-sided $p<0.05$ was considered significant.

Results

Patient cohort

We retrospectively collected the clinical and CT image data of 764 TB patients (DR-TB, $n=164$; DS-TB, $n=600$) who were diagnosed through sputum culture and have completed drug-susceptibility testing from April 2018 to December 2020. We excluded a large proportion of cases according to exclusion criteria. Finally, 177 cases (DR-TB, $n=78$; DS-TB, $n=99$) were remained in the study. (Fig. 2)

We performed a descriptive statistical analysis of the demographic data, clinical symptoms, laboratory examination indicators and imaging characteristics of 177 patients with PTB. The results are displayed in Tables 1 and 2. The result of univariate regression analyses (Table 3) revealed that history of diabetes, pulmonary exudation, pulmonary proliferation, fibrosis, number of lung lobes involved by cavities, type of cavity wall and number of cavities were significantly different between the DR-PTB and DS-PTB.

Construction of the clinical model

The multivariable logistic regression analysis (Table S1) showed that history of diabetes, pulmonary exudation, pulmonary proliferation, fibrosis, type of cavity wall can help to differentiate DR-TB from DS-TB. The clinical factor model showed AUC 0.780 (95% CI 0.700–0.859), sensitivity 55.2%, specificity 86.4%, accuracy 71.8% in the training set, while the validation set showed similar results (0.692 (95% CI 0.546–0.839), 45.0%, and 78.8%, and66%, respectively) (Table 4). The ROC curves were showed in Fig. 3. The clinical factor model is less effective in the differential diagnosis of DR-PTB and DS-PTB.

Radiomics feature extraction and construction of the radiomics signature

We extracted 833 radiomics features from all patients' CT lung window images based on two kinds of image preprocessing method, and used LASSO to screen out 13 valuable predictive features, so as to use logical regression to construct radiomics signature after dimension reduction.

We used five-fold cross validation to screen the super parameters γ in LASSO logistic regression model. (Figure S1) The Rad-score was calculated using the following formula: Radscore=-15.091864+0.007245×original_ngtdm_Busyness-3.866186×original_shape_Flatness+0.079206×wavelet. HHH_firstorder_Kurtosis.

+ 3.774584×wavelet.HHH_glcm_Idn×-6.20E-05×wavelet.HHH_ngtdm_Busyness-0.025882×wavelet.HLL_ngtdm_Busyness + 1.662739×wavelet.LHH_firstorder_Mean-63.03919×wavelet.LHH_glcm_Imc1 + 1.151943×wavelet.LHH_glszm_ZoneEntropy + 0.311706×wavelet.LLH_gldm_DependenceEntropy + 0.315799×wavelet.LLH_gldm_DependenceEntropy+0.002307×wavelet.LLL_glcm_DifferenceVariance-0.078382×wavelet.LLL_ngtdm_Strength.

Figure S2 showed the Rad-scores of each patient in the training set and validation set. The Rad-score showed statistically significant difference between DR-PTB and

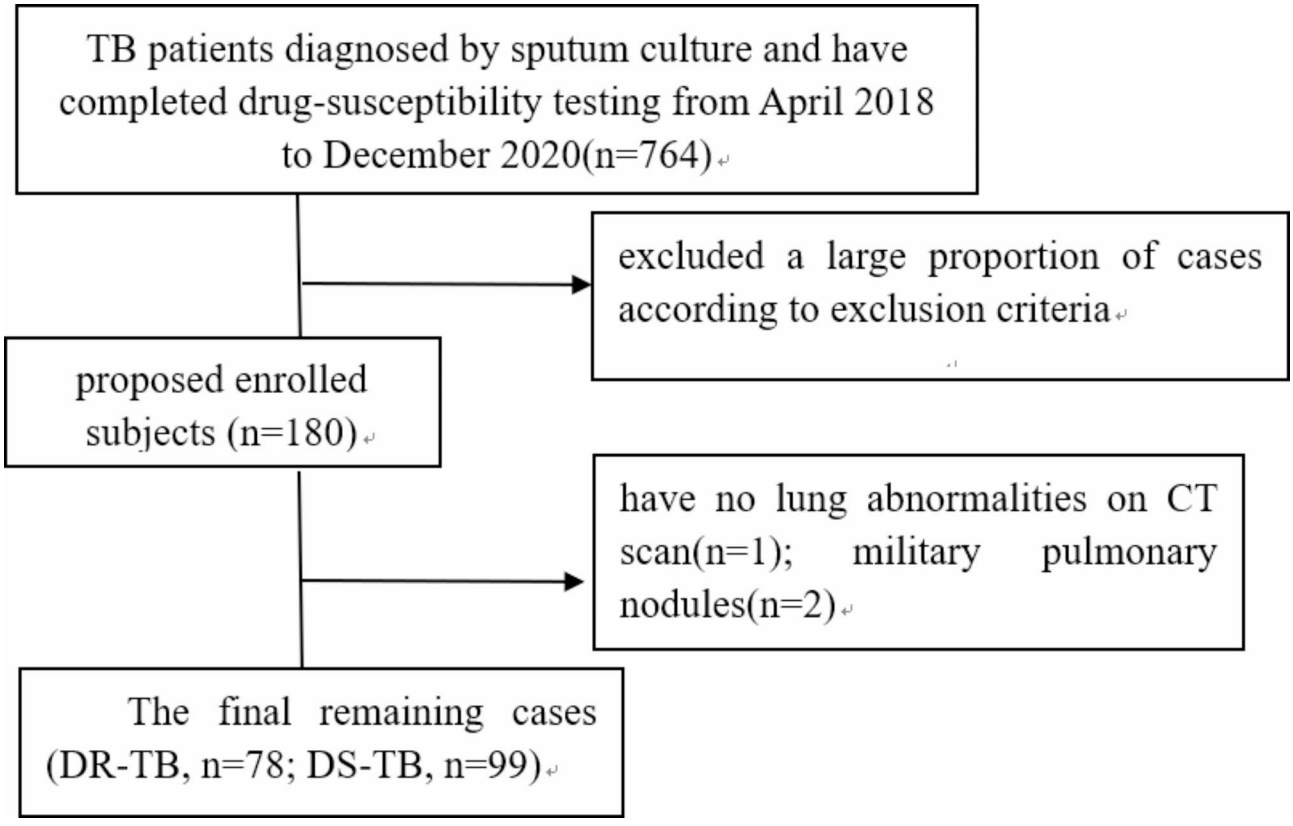

Fig. 2 Flow chart of patient cohort

DS-PTB ($P<0.01$; OR(95%CI). 16.424(6.779,48.235)). The radiomics signature showed good discrimination in the training set (AUC, 0.891; 95% CI, 0.832～0.951; sensitivity, 82.8%;specificity, 86.4%; accuracy,84.7%) and the validation set (AUC, 0.803;95% CI, 0.674～0.932; sensitivity, 70.0%;specificity, 69.7%; accuracy,69.8%). (Fig. 4)

Construction of a combined model with clinical factors and rad-score

We enrolled the rad-score, history of diabetes, pulmonary exudation, pulmonary proliferation, fibrosis, and type of cavity wall as predictors in a logistic regression analysis (Table 5) to develop the radiomics-clinical nomogram. The Nomo-score was calculated using the following formula: Nomo-score=2.64×history of diabetes −2.3×pulmonary exudation+1.693×pulmonary proliferation+1.129×fibrosis+1.034×thick-walled cavity −0.179×thin-walled or worm-eaten cavity+3.04×Rad-score. Figure 6 showed the calibration curve of the radiomics-clinical model. The predicted probability of the nomogram is in good agreement with the actual probability (Fig. 5). Radiomics-clinical model was visualized as the nomogram. Table 4; Fig. 6 showed that AUC, accuracy, specificity and sensitivity of the nomogram of the radiomics-clinical model have improved to a certain extent. The radiomics-clinical model showed good calibration and discrimination in the training set (AUC, 0.932;95% CI, 0.888–0.977; sensitivity, 86.2%; specificity; 90.9%; accuracy, 88.7%) and the validation set (AUC, 0.841; 95% CI, 0.719～0.962; sensitivity, 75.0%; specificity;78.8%; accuracy,77.4%). This suggested that the radiomic features have an important value in differentiating drug resistance of pulmonary tuberculosis.

Clinical application

The decision curve analysis for the radiomics signature, the clinical model and the radiomics-clinical nomogram (Fig. 7) are shown in Fig. 8. The decision curve analysis showed that across the majority of the range of reasonable threshold probabilities, the radiomics-clinical model had a higher overall benefit than the clinical factor model and radiomics signature in distinguishing DS-PTB and DR-PTB.

Discussion

The emergence and spread of resistant tuberculosis pose a serious threat to global TB control. Patients with DR-PTB, if not diagnosed and managed on time, will lead to poor treatment and disease transmission. Chest CT scanning is of great significance in imaging diagnosis, differential diagnosis and efficacy evaluation of DR-PTB, and it is also widely used in clinical practice. However,

Table 1 Demographic data, clinical symptoms, laboratory examination indicators of DS-PTB and DR-PTB

feature parameters	training sets($n=124$)			validation sets($n=53$)		
	DS-PTB	DR-PTB	P value	DS-PTB	DR-PTB	P value
age	35 (24, 60)	48.5(28.3, 57.6)	0.246	31(25, 58)	49(43, 59.5)	0.1
gender (%)	40(60.6)	39(67.2)	0.562	21(63.6)	15(75.0)	0.579
male	26(39.4)	19(32.8)		12(36.4)	5(25.0)	
female						
diabetes(%)	63(95.5)	48(82.8)	0.045	31(93.9)	15(75.0)	0.12
no	3(4.5)	10(17.2)		2(6.1)	5(25.0)	
yes						
Diagnosistypes(%)	56(84.8)	45(77.6)	0.42	29(87.9)	13(65.0)	0.101
initial treatment	10(15.2)	13(22.4)		4(12.1)	7(35.0)	
retreatment						
Cough and sputum (%)	14(21.2)	9(15.5)	0.021	7(21.2)	2(10)	0.241
no	52(78.8)	49(84.5)		26(78.8)	18(90)	
yes						
hemoptysis (%)	56(84.8)	46(79.3)	0.569	31(93.9)	17(85)	0.552
no	10(15.2)	12(20.7)		2(6.1)	3(15)	
yes						
fatigue (%)	60(90.9)	49(84.5)	0.413	31(93.9)	19(95)	<0.9
no	6(9.1)	9(15.5)		2(6.1)	1(5)	
yes						
emaciation (%)	64(97.0)	52(89.7)	0.198	32(97)	18(90)	0.652
no	2(3.0)	6(10.3)		1(3)	2(10)	
yes						
night sweats (%)			<0.9			<0.9
no	61(92.4)	53(91.4)		31(93.9)	18(90)	
yes	5(7.6)	5(8.6)		2(6.1)	2(10)	
chest tightness and shortness of breath (%)			0.943			0.681
no	56(84.8)	48(82.8)		27(81.8)	18(90)	
yes	10(15.2)	10(17.2)		6(18.2)	2(10)	
fever (%)			0.039			0.252
no	40(60.6)	46(79.3)		22(66.7)	17(85)	
yes	26(39.4)	12(20.7)		11(33.3)	3(15)	
sedimentation rate (mm/H)	28(6.25, 57)	11.5(5, 30)	0.023	21(6, 44)	23(13, 58.2)	0.255
C reactive protein (mg/L)	9.5(4, 34.5)	9(7, 19.9)	0.698	6.10(4, 33.6)	9(6.7, 24.9)	0.279

differential diagnosis remains challenging because of the overlap in imaging features between DS-PTB and DR-PTB [7–9]. Our study showed that the AUC of the comprehensive model based on CT scan combined with Rad-score and clinical factors in training set and validation set is 0.932 and 0.841 respectively, which had good predictive value. The decision curve analysis showed that across the majority of the range of reasonable threshold probabilities, the radiomics-clinical model had a higher overall benefit than the clinical model and radiomics signature in distinguishing DS-PTB and DR-PTB. This indicated that radiomic features, clinical factors and CT imaging signs had a high degree of complementarity, providing a new idea for radiomics research.

The multivariable logistic regression analysis of radiomics-clinical showed that the OR of diabetes, proliferation, fibrosis, thick-walled cavity and Rad score was greater than 1, which was a risk factor, while pulmonary exudation and thin-walled or worm-eaten cavities are protective factors. What is more, diabetes, pulmonary exudation, Rad score were independent predictors of DR-PTB. It is suggested that the diagnosis of DR-PTB is more likely when thick -walled cavities, proliferative lesions and fibrosis appear. Previous studies pointed out that DS-PTB and DR-PTB can all have cavities, and DR-PTB is more often manifested as multiple cavities, especially ≥3 cavities, and thick walled-cavities, and lesions involving a wide range [14]. C et al. [15] pointed out that thick -walled cavity was statistically different between the two groups and was an independent risk factor for DR-PTB. However, the study of SONG et al. [16] pointed out that in patients with type 2 diabetes, there was no statistical difference in the distribution of multiple cavities in DR and DS -PTB. It was speculated that the reason may be related to the different sizes of cavities, some of which are large, some of which are surrounded by exudation and consolidation, and even some smaller cavities are merged with each other, resulting in unclear boundaries and hard to count. We also found this phenomenon in the image evaluation, so when setting the dummy

Table 2 Imaging characteristics of DS-PTB and DR-PTB

imaging features	**training set($n=124$)(%)**			**validation sets($n=53$)(%)**		
	DS-PTB	DR-PTB	P value	DS-PTB	DR-PTB	P value
number of lung lobes involved			0.177			0.134
1	13(19.7)	6(10.3)		5(15.2)	2(10)	
2	13(19.7)	8(11.5)		8(24.2)	1(5)	
≥ 3	40(60.6)	44(78.2)		20(60.6)	17(85)	
emphysema			0.136			0.211
no	57(86.4)	43(74.1)		29(87.9)	14(70)	
yes	9(13.6)	15(25.9)		4(12.1)	6(30)	
atelectasis			0.288			0.798
no	65(98.5)	54(93.1)		33(100)	19(95)	
yes	1 (1.5)	4(6.9)		0(0)	1(5)	
bronchial wall thickening			0.131			0.107
no	22(33.3)	28(48.3)		17(51.5)	5(25)	
yes	44(66.7)	39(51.7)		16(48.5)	15(75)	
bronchiectasis			0.126			0.003
no	34(51.5)	21(36.2)		25(75.8)	6(30)	
yes	32(48.5)	37(63.8)		8(24.2)	14(70)	
bronchial dissemination			0.095			0.096
no	36(54.5)	22(37.9)		19(57.6)	6(30)	
yes	30(45.5)	36(62.1)		14(42.4)	14(70)	
pulmonary exudation			0.071			0.833
no	6(9.1)	13(22.4)		3(9.1)	3(15)	
yes	60(90.9)	45(77.6)		30(18.2)	17(85)	
pulmonary proliferation			0.012			0.339
no	15 (22.7)	3(5.2)		6(18.2)	1(5)	
yes	51(77.3)	55(94.8)		27(81.8)	19(95)	
fibrosis			<0.001			0.206
no	50(75.8)	25(43.1)		22(66.7)	9(45)	
yes	16(24.2)	33(56.9)		11(33.3)	11(55)	
pleural effusion			0.298			0.279
no	58(87.9)	55(94.8)		29(87.9)	20(100)	
yes	8(12.1)	3(5.2)		4(12.1)	0(0)	
pleural thickening with calcification			0.706			0.288
no	63(95.5)	57(98.3)		32(97)	17(85)	
yes	3(4.5)	1(1.7)		1(3)	3(15)	
pleural thickening			0.172			<0.9
no	48(72.7)	49(84.5)		26(78.8)	16(80)	
yes	18(27.3)	9(15.5)		7(21.2)	4(20)	
collapsed thoracic cages			<0.9			0.652
no	63(95.5)	56(96.6)		32(97)	18(90)	
yes	3(4.5)	2(3.4)		1(3)	2(10)	
nodule or mass			0.733			0.269
no	58(87.9)	53(91.4)		31(93.9)	16(80)	
yes	8(12.1)	5(8.6)		2(6.1)	4(20)	
calcification			0.136			0.405
no	57(86.4)	43(74.1)		29(87.9)	15(75)	
yes	9(13.6)	15(25.9)		4(12.1)	5(25)	
type of cavity wall			0.007			0.129
thick-walled cavity	26(39.4)	39(67.2)		15(45.5)	11(55)	
thin-walled or worm-eaten cavity	6(9.1)	2(3.4)		2(6.1)	4(20)	
cavity with fluid plane			<0.9			0.093
no	65(98.5)	57(98.3)		33(100)	17(85)	
yes	1(1.5)	1(1.7)		0(0)	3(15)	

Table 2 (continued)

imaging features	training set($n=124$)(%)			validation sets($n=53$)(%)		
cavity with calcification			0.907			<0.9
no	60(90.9)	54(93.1)		31(93.9)	19(95)	
yes	6(9.1)	4(6.9)		2(6.1)	1(5)	
number of lung lobes involved by cavities			0.041			0.19
0	34 (51.5)	17(29.3)		16(48.5)	5(25)	
1	20(30.3)	24(41.4)		11(33.3)	8(40)	
≥ 2	12(18.2)	17(29.3)		6(18.2)	7(35)	
number of cavities			0.041			0.136
0	34(50.5)	17(28.2)		16(48.5)	5(25)	
1	16(22.2)	19(34.6)		6(18.2)	8(40)	
≥ 2	16(27.3)	22(37.2)		11(33.3)	7(35)	

Note Figures are numbers (percentages) of patients unless stated otherwise, the rest are median and quartile [M(P25, P75)]

variable of the number of cavities, we counted the number of 2 or more cavities. In addition, in the multivariate logistic regression analyses, the number of cavities and lung lobes involved by cavities have multiple collinearity and are excluded from the clinical model. The imaging manifestations of the exudative lesions included single or multiple patchy, cloud -like ground glass lesions with slightly higher density, varying sizes, uneven density, and blurred edges when the lesions were in exudative lesions. When the lesions progressed into the consolidation phase, the attenuation appeared as a homogeneous increase. Lee et al. [17] noted that patients with extensive DR-PTB were more likely to see extensive consolidation in chest CT scan. Shin et al. [18] also proposed that chest CT of multidrug resistant TB patients were more likely to see consolidation from lung segment to lung lobe. Our research pointed out that the distribution of exudative lesions between the two groups was statistically different, which was a protective factor of drug-resistant pulmonary tuberculosis, and was consistent with the results of Cheng et al. [9]. We speculate that the reasons are as follows: First, drug-sensitive pulmonary tuberculosis usually has a good response to anti tuberculosis drugs, and timely and effective treatment may lead to rapid absorption and reduction of lesions. This may lead to more exudative lesions on imaging. Second, patients with drug sensitive pulmonary tuberculosis may experience increased inflammatory response in lung tissue due to the death of *Mycobacterium tuberculosis* and the action of antibiotics after receiving anti tuberculosis drug treatment, leading to worsening of exudative lesions. Third, anti-tuberculosis drug therapy may activate the patient's immune system, and enhance the clearance of immune cells against *Mycobacterium tuberculosis*, thereby further exacerbating the inflammatory response and leading to the formation of exudative lesions. The pulmonary proliferation of TB is a granulomatous lesion, which is mainly formed by filling and obstructing the drainage bronchus with caseating necators. Pulmonary proliferation is generally manifested as well-circumscribed multiple nodules, and the lesion is clustered but without fusion signs. Our research pointed out that the proliferation have statistical significance between the two groups, which is consistent with the literature [9]. Our study also pointed out that there was statistically significant difference between the two groups in fibrosis. We speculate that it may be because PTB patients are prone to fibrosis after anti tuberculosis treatment [19]. In addition, DR-PTB patients have been treated for a long time, and the exudation and consolidation in the lungs of patients are not easy to be absorbed, so the lesion turns to fibrosis and pulmonary tissue atrophy. However, few studies have evaluated the difference in fibrosis between the two groups.

Clinical signs and symptoms of adults infected with PTB are not specific [20, 21]. A meta-analysis indicated that diabetes is an independent risk factor for DR-PTB, which may be related to metabolic changes and immune impairment in patients with TB and diabetes [22, 23]. In the radiomics-clinical multivariate logistic regression analysis, it can be seen that history of diabetes is an independent predictor of DR-PTB.

Radiomics refers to high-throughput extraction and analysis of a large number of advanced and quantitative imaging features from medical imaging images such as CT, PET or MRI [24]. Currently, the application of radiomics in pulmonary TB is differential diagnosis with single lesion such as mass cryptococcus, and pulmonary adenocarcinoma [11, 12]. However, it has also been used in the differential diagnosis of non-tuberculosis mycobacterium [25]. Therefore, we boldly propose the hypothesis that radiomics can be used to differentiate DR-PTB and DS-PTB with multiple and multiple types lesions. After screening the features, a total of 13 radiomic features were obtained. Wavelet transform is the most commonly used texture analysis method at present and wavelet texture features are superior to other features [26]. 11 radiomic parameters in our results are wavelet

Variable	OR (95%CI)	P-value
gender		
male	1.0	
female	0.75(0.355,1.563)	0.444
age	1.01(0.992,1.029)	0.288
diagnosis types		
initial treatment	1.0	
retreatment	1.618(0.652,4.12)	0.302
diabetes		
no	1.0	
yes	4.375(1.259,20.307)	0.031
cough and sputum		
no	1.0	
yes	1.892(0.745,5.011)	0.185
hemoptysis		
no	1.0	
yes	1.461(0.579,3.756)	0.422
fatigue		
no	1.0	
yes	1.837(0.619,5.815)	0.279
emaciation		
no	1.0	
yes	3.692(0.812,25.928)	0.119
fever		
no	1.0	
yes	1.566(0.540,4.534)	0.409
chest tightness and shortness of breath		
no	1.0	
yes	1.167(0.443,3.074)	0.752
night sweats		
no	1.0	
yes	1.151(0.305,4.347)	0.831
C reactive protein	0.992(0.975,1.007)	0.3
erythrocyte sedimentation rate	1.639(0.703,3.821)	0.253
number of lung lobes involved		
1	1.0	
2	1.333(0.361,5.103)	0.666
≥3	2.383(0.856,7.334)	0.108
emphysema		
no	1.0	
yes	2.209(0.897,5.713)	0.09
atelectasis		
no	1.0	
yes	4.815(0.687,95.697)	0.165
bronchial wall thickening		
no	1.0	
yes	0.536(0.257,1.103)	0.092
bronchiectasis		
no	1.0	
yes	1.872(0.916,3.888)	0.088
bronchial dissemination		
no	1.0	
yes	1.964(0.963,4.068)	0.066
pulmonary exudation		
no	1.0	
yes	0.346(0.114,0.947)	0.046
pulmonary proliferation		
no	1.0	
yes	5.392(1.661,24.263)	0.011
fibrosis		
no	1.0	
yes	4.125(1.946,9.059)	<0.001
calcification		
no	1.0	
yes	2.209(0.897,5.713)	0.09
nodule or mass		
no	1.0	
yes	0.684(0.196,2.18)	0.527
number of cavities		
no	1.0	
1	2.375(0.989,5.839)	0.055
≥2	2.75(1.167,6.672)	0.022
number of lung lobes involved by cavities		
no	1.0	
1	2.4(1.054,5.596)	0.039
≥2	2.833(1.119,7.422)	0.03
type of cavity wall		
no	1.0	
thick-walled cavity	3(1.413,6.558)	0.005
thin-walled or worm-eaten cavity	0.667(0.091,3.258)	0.641
cavity with fluid plan		
no	1.0	
yes	1.14(0.044,29.278)	0.927
cavity with calcification		
no	1.0	
yes	0.741(0.181,2.731)	0.655
pleural effusion		
no	1.0	
yes	0.395(0.083,1.445)	0.187
pleural thickening with calcification		
no	1.0	
yes	0.368(0.018,2.969)	0.393
pleural thickening		
no	1.0	
yes	0.49(0.193,1.173)	0.117
collapsed thoracic cages		
no	1.0	
yes	0.75(0.096,4.681)	0.757

Table 3 Univariate regression analyses of clinical and imaging characteristics of DS-PTB and DR-PTB

feature images, which shows that wavelet transform features play an important role in prediction models. In fact, a single radiomic feature is not enough to represent the heterogeneity of tissues, and cannot reflect the overall characteristics of the lesions [27]. It is necessary to combine different radiomic parameters. The potential difference between drug sensitive and drug resistant pulmonary tuberculosis can be distinguished by combining the above 13 radiomics features.

This study explored the differential diagnostic value of radiomics features in pulmonary tuberculosis by extracting massive amounts of information from images and establishing models. Combined with the Rad-score and clinical factors, a radiomics-clinical model nomogram was constructed. Compared with those of the other two models, the diagnostic efficiency of the comprehensive model is improved, and clinical doctors are more receptive to more intuitive and objective radiomics-clinical nomogram, which can be well applied in clinical practice. Unlike previous studies that only extract radiomics features based on certain imaging features, this study not only extracted semantic features and evaluated the differences in chest imaging performance between two groups, but also outlined ROI that covers all imaging features, including exudation, proliferation, cavities, etc., which can comprehensively measure the drug resistance of pulmonary tuberculosis.

This study has several limitations. Firstly, the study is a retrospective study. The sample size of our study is small and the research object is from the same institution. Thus, there is a selection bias and a risk of overfitting the model. Therefore, future studies can collect data from multiple centers to expand the sample size. Secondly, precise segmentation of lesions is very important for radiomic feature extraction and model construction and is the most critical, challenging and controversial part in radiomics [28]. Subsequent radiomic features are extracted from the segmented volume. The ROI segmented in this study covered all CT image features, including exudation, proliferation, bronchiectasis, etc., which can comprehensively evaluate the severity and scope of lung injury. Although the accuracy is high, the pulmonary tuberculosis image is complex and is time-consuming and difficult to sketch lesions. In addition, there is a strong subjectivity problem for CT image evaluation, so it is necessary to develop a reliable and repeatable automatic segmentation method. Thirdly, at present, the focus of radiomics analysis is to improve the prediction ability of the model rather than to explain the biological interpretation of the radiomic features, which is not completely clear and needs further discussion.

Conclusions

In conclusion, a simple radiomics signature is of great value in differentiating DS-PTB and DR-PTB. The radiomics-clinical model nomogram shows a good prediction effect, which may help clinicians to formulate precise treatment. This study explored and proved the value of radiomics in the differential diagnosis of drug resistance of pulmonary tuberculosis, and also proved

Table 4 Comparison of diagnostic performance of clinical model, radiomics signature and radiomics-clinical model in training set and validation set

Model	Accuracy	Sensitivity	Specificity	AUC	95%CI
Radiomics-clinical model _train	0.887	0.862	0.909	0.932	0.888～0.977
Radiomics-clinical model _ validation	0.774	0.75	0.788	0.841	0.719～0.962
Radiomics model _train	0.847	0.828	0.864	0.891	0.832～0.951
Radiomics model _ validation	0.698	0.700	0.697	0.803	0.674～0.932
Clinical model_train	0.718	0.552	0.864	0.780	0.700～0.859
Clinical model_ validation	0.660	0.450	0.788	0.692	0.546～0.839

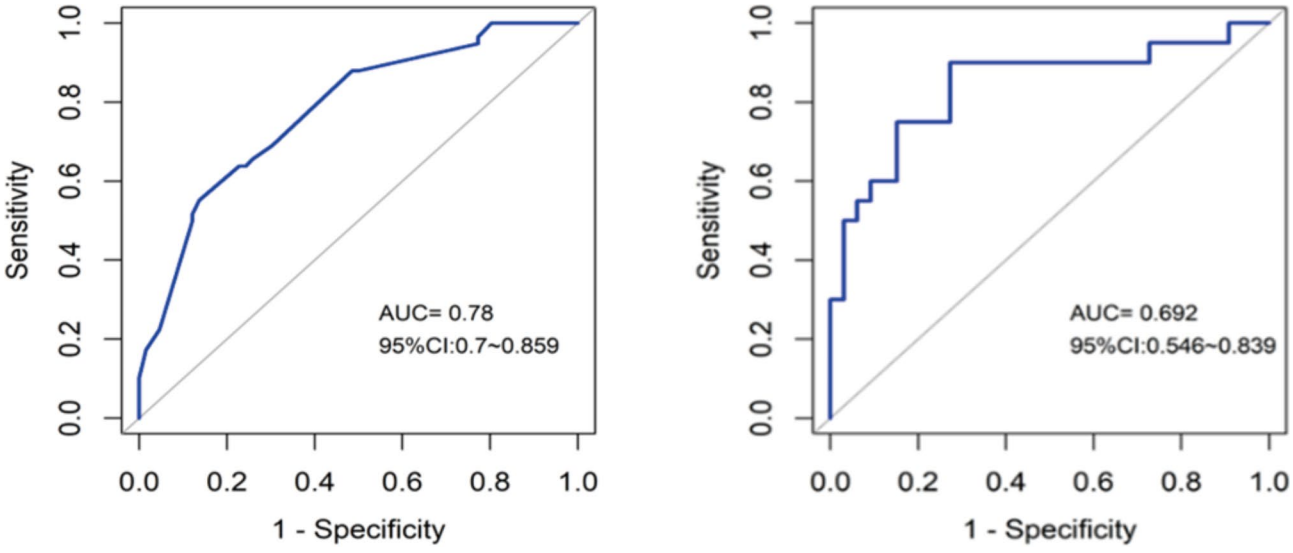

Fig. 3 In clinical model, AUC of training set is 0.780(95% CI, 0.700～0.859), while AUC of validation set is 0.692(95% CI, 0.546～0.839)

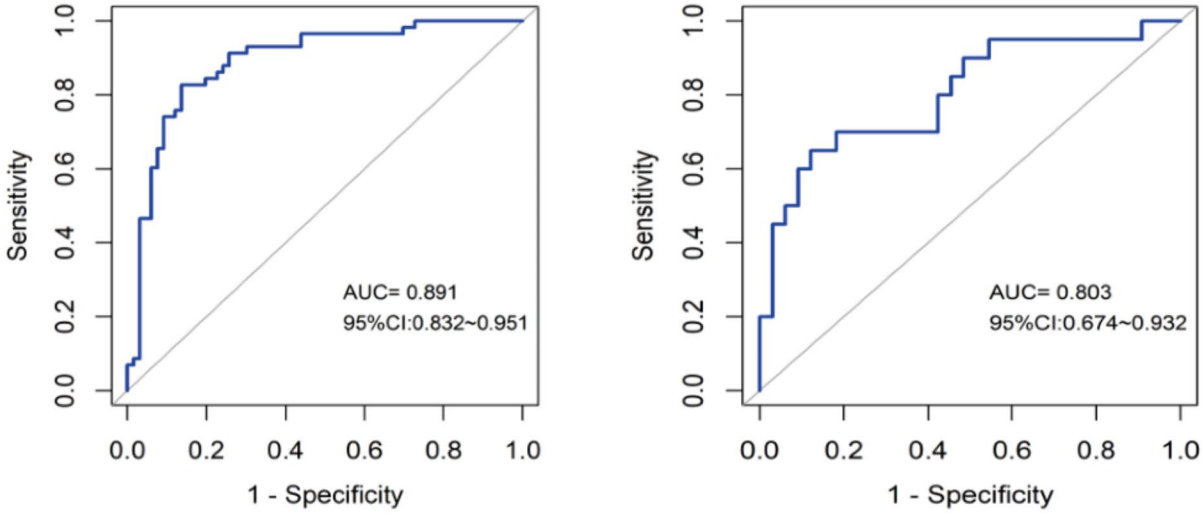

Fig. 4 The AUC of the training set of radiomics signature is 0.891, and the AUC of the validation set is 0.803

the potential of radiomics in the diagnosis and differential diagnosis of non-neoplastic pulmonary conditions, providing new ideas for the research of pulmonary infectious diseases.

Table 5 The multivariable logistic regression analysis of radiomics-clinical for influencing factors of drug resistance in pulmonary tuberculosis

variable	OR	95%CI	*P*
history of diabetes	14.016	1.931,130.779	0.012
pulmonary exudation	0.1	0.01,0.706	0.032
pulmonary proliferation	5.438	0.843,51.005	0.097
fibrosis	3.093	0.993,10.329	0.056
thick-walled cavity	2.811	0.865,9.865	0.092
thin-walled or worm-eaten cavity	0.836	0.079,7.48	0.873

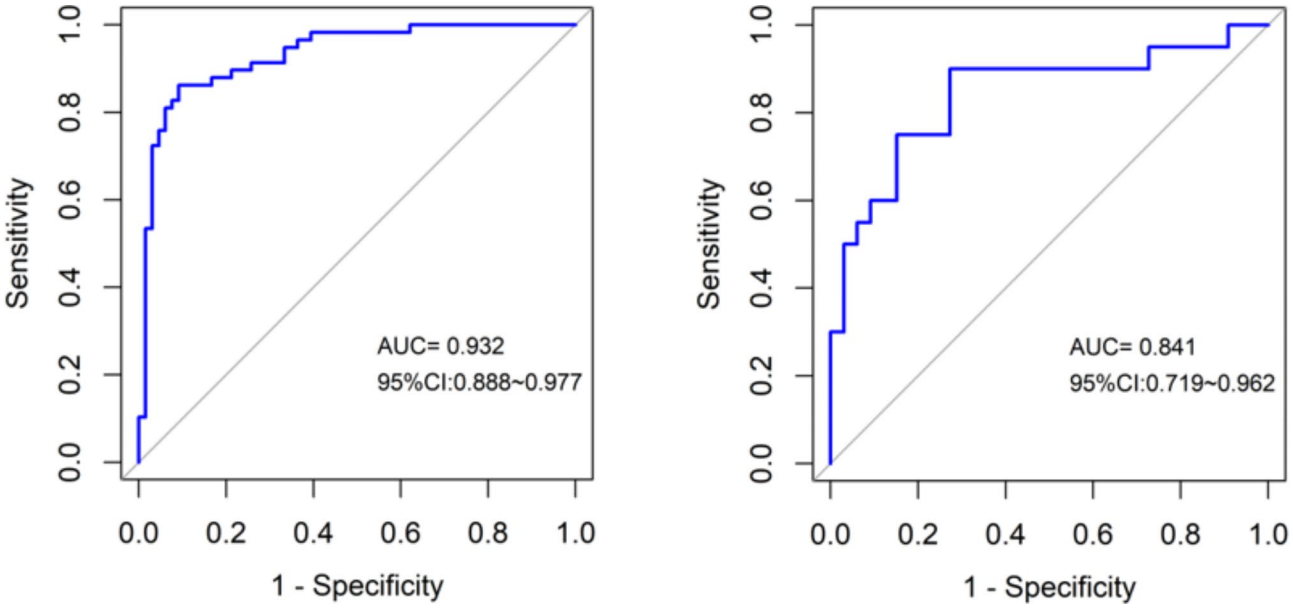

Fig. 6 The AUC of the training set of the radiomics-clinical model was 0.932, and the AUC of the validation set was 0.841

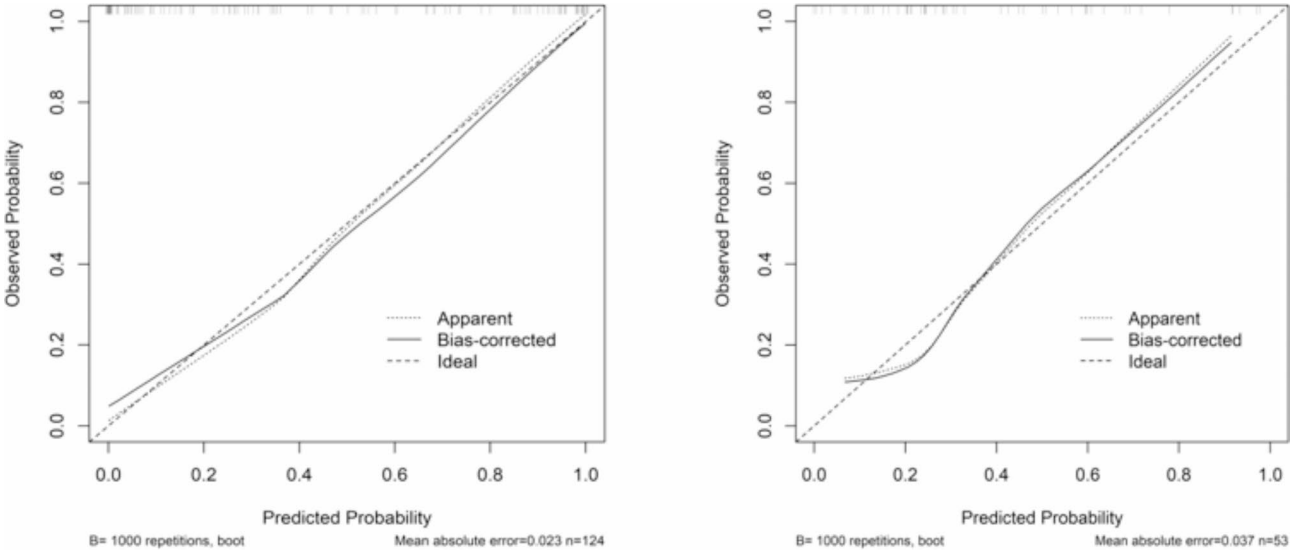

Fig. 5 The calibration curve of the radiomics-clinical model drawn by using bootstrap with 1000 resamples. The abscissa is the predicted probability of the model, and the ordinate is the observed probability. Ideal line represents the reference curve, apparent line is the uncalibrated probability curve, and bias -corrected line is the calibrated probability curve. The closer the calibration curve is to the reference curve, the better the model consistency. The left figure is the calibration curve of the training set, while the right figure is the calibration curve of the validation set. The calibration curve shows a good agreement between the actual probability and the predicted probability

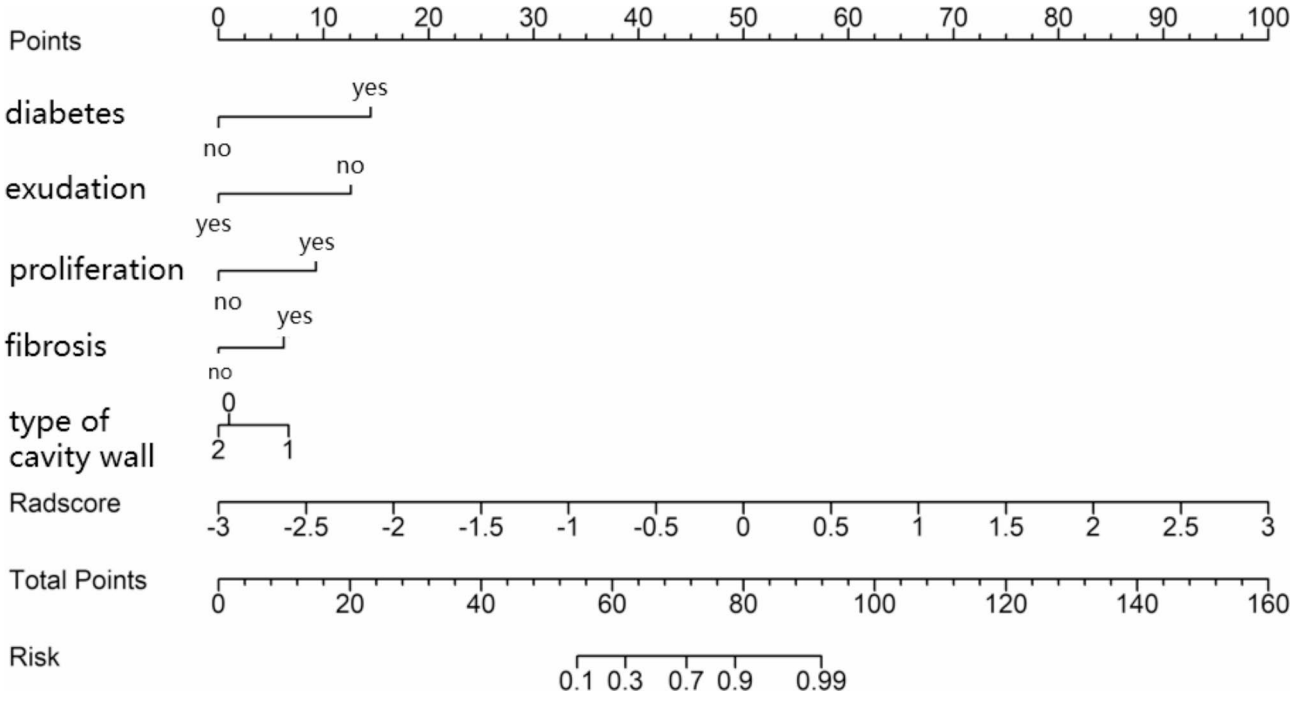

Fig. 7 The radiomics-clinical nomogram. Each included variable corresponds to the corresponding score, and the sum of the scores of each variable is the total score. The higher the total score, the higher the probability of predicting drug resistance of pulmonary tuberculosis. Note: 0, 1 and 2 in the type of cavity wall are respectively no cavity, thick-walled cavity, thin-walled or worm-eaten cavity

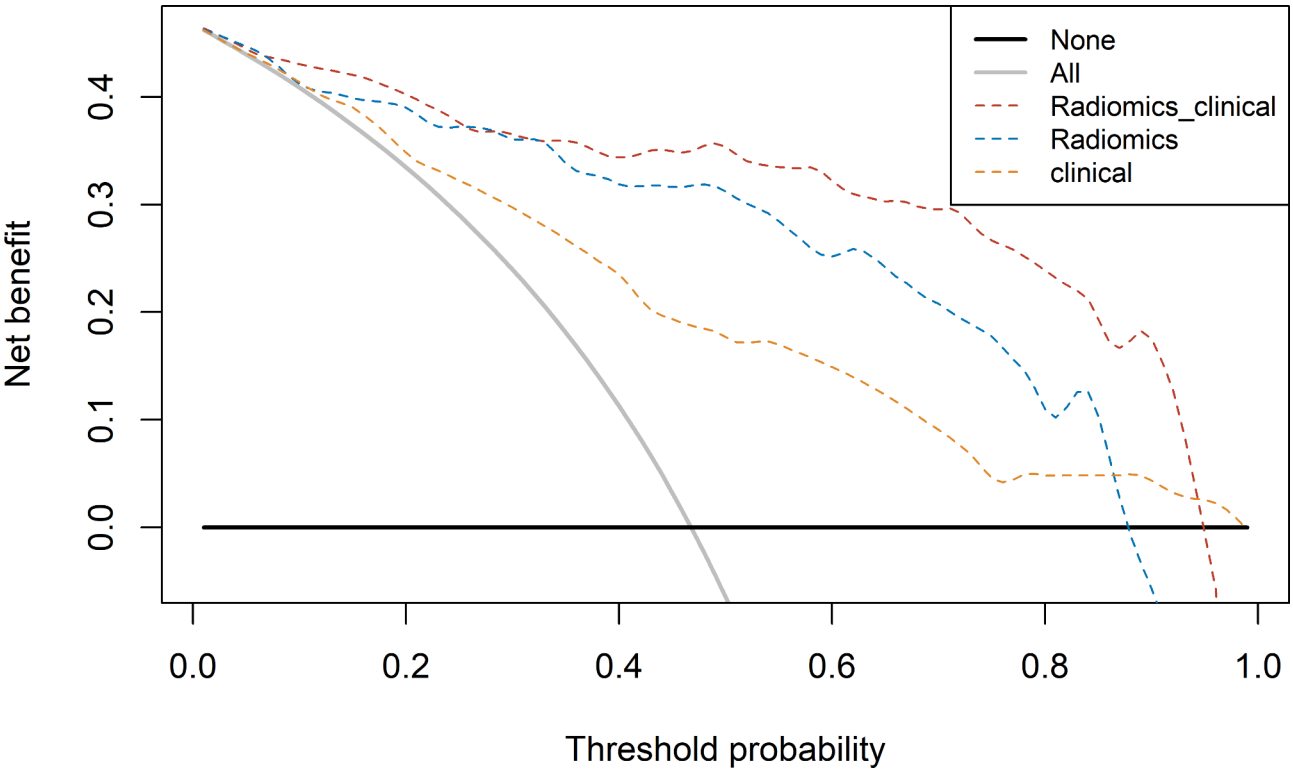

Fig. 8 Decision curve analysis for three models. The y-axis indicates the net benefit and x-axis indicates threshold probability. Red, blue and orange represent the net benefit of radiomics-clinical model, the radiomics signature and the clinical model respectively. Obviously, the radiomics-clinical nomogram was better than radiomics signature and clinical model with added net benefit

Abbreviations

CT	Computed tomography
TB	Tuberculosis
DR-PTB	Drug-resistant pulmonary tuberculosis
DS-PTB	Drug-sensitive pulmonary tuberculosis
AUC	Area under the curve
95%CI	95% confidence interval
WHO	World Health Organization
CRP	C reactive protein
ESR	Erythrocyte sedimentation rate
ROI	Region of interest
LASSO	Least absolute shrinkage and selection operator
ROC	Receiver operating characteristic curve
DCA	Decision curve analysis

Supplementary Information

The online version contains supplementary material available at https://doi.org/10.1186/s12880-024-01481-4.

Supplementary Material 1

Acknowledgements
Not applicable.

Author contributions

Authors and Affiliations Department of Radiology, Zhongda Hospital, Medical School, Southeast University, 87 Dingjiaqiao Road, Nanjing 210009, China. Department of Radiology, Zhejiang Cancer Hospital, Hangzhou 310022, ChinaFeng-li Jiang Department of Radiology, Zhongda Hospital, Medical School, Southeast University, 87 Dingjiaqiao Road, Nanjing 210009, China. Yu Wang, Qiu-zhen Xu Department of Radiology, The Second Hospital of Nanjing, Nanjing University of Chinese Medicine, Nanjing city, Jiangsu province 210003, China Chuan-jun Xu Contributions Designed: FLJ, CJX; Data curation: FLJ; Formal analysis: FLJ, YW; Methodology: FLJ, CJX; Software: FLJ, QZX; Writing-original draft: FLJ; Writing-review & editing: FLJ, QZX. All authors read and approved the final manuscript. Corresponding author Correspondence to Qiu-zhen Xu.

Funding
This work was supported by grants from Infectious and Inflammatory Radiology Committee of Jiangsu Research Hospital Association (2022-FS-01-001and2022-FS-01-002),Nanjing Medical Science and technique Development Foundation(YKK21126),and Jiangsu Medical Association Lunqin Imaging Research Special Fund Project (SYH-3201150-0009(2021004)). The funding bodies played no role in the design of the study and collection, analysis, and interpretation of data and in writing the manuscript.

Data availability
No datasets were generated or analysed during the current study.

Declarations

Ethics approval and consent to participate
The ethics committee of The Second Hospital of Nanjing (No. 2023-LY-kt106). approved this retrospective study with a waiver of informed consent because the study was an observational, retrospective study using a database from which the patients' identifying information had been removed.

Consent for publication
Not applicable.

Competing interests
The authors declare no competing interests.

Received: 9 December 2023 / Accepted: 24 October 2024
Published online: 12 November 2024

References

1. Luies L, du Preez I. <ArticleTitle Language="En">The Echo of Pulmonary Tuberculosis: mechanisms of clinical symptoms and other Disease-Induced systemic complications. Clin Microbiol Rev. 2020;33(4):e00036–20.
2. Global tuberculosis report 2021. Geneva: World Health Organization. 2021.
3. Nahid P, Mase SR, Migliori GB, Sotgiu G, Bothamley GH, Brozek JL, et al. Treatment of Drug-Resistant Tuberculosis. An Official ATS/CDC/ERS/IDSA Clinical Practice Guideline. Am J Respir Crit Care Med. 2019;200(10):e93–142.
4. Suárez I, Fünger S, Kröger S, Rademacher J, Fätkenheuer G, Rybniker J. The Diagnosis and Treatment of Tuberculosis. Dtsch Arztebl Int. 2019;116(43):729–35.
5. Tornheim J, Starks A, Rodwell T, Gardy J, Walker T, Cirillo D, et al. Building the Framework for Standardized Clinical Laboratory Reporting of Next-generation Sequencing Data for Resistance-associated Mutations in Mycobacterium tuberculosis Complex. Clin Infect Dis. 2019;69(9):1631–3.
6. Van Rie A, Enarson D. XDR tuberculosis: an indicator of public-health negligence. Lancet. 2006;368(9547):1554–6.
7. Wáng Y, Chung M, Skrahin A, Rosenthal A, Gabrielian A, Tartakovsky M. Radiological signs associated with pulmonary multi-drug resistant tuberculosis: an analysis of published evidences. Quant Imaging Med Surg. 2018;8(2):161–73.
8. Li D, He W, Chen B, Lv P. Primary multidrug-resistant tuberculosis versus drug-sensitive tuberculosis in non-HIV-infected patients: Comparisons of CT findings. PLoS ONE. 2017;12(6):e0176354.
9. Cheng N, Wu S, Luo X, Xu C, Lou Q, Zhu J, et al. A Comparative Study of Chest Computed Tomography Findings: 1030 Cases of Drug-Sensitive Tuberculosis versus 516 Cases of Drug-Resistant Tuberculosis. Infect Drug Resist. 2021;14:1115–28.
10. Lambin P, Rios-Velazquez E, Leijenaar R, Carvalho S, van Stiphout R, Granton P, et al. Radiomics: extracting more information from medical images using advanced feature analysis. Eur J cancer. 2012;48(4):441–6.
11. Feng B, Chen X, Chen Y, Lu S, Liu K, Li K, et al. Solitary solid pulmonary nodules: a CT-based deep learning nomogram helps differentiate tuberculosis granulomas from lung adenocarcinomas. Eur Radiol. 2020;30(12):6497–507.
12. Wei S, Shi B, Zhang J, Li N. Differentiating mass-like tuberculosis from lung cancer based on radiomics and CT features. Transl Cancer Res. 2021;10(10):4454–63.
13. Song Y, Zhang J, Zhang Y, Hou Y, Yan X, Wang Y, et al. FeAture Explorer (FAE): A tool for developing and comparing radiomics models. PLoS ONE. 2020;15(8):e0237587.
14. Yeom J, Jeong Y, Jeon D, Kim K, Kim C, Park H, et al. Imaging findings of primary multidrug-resistant tuberculosis: a comparison with findings of drug-sensitive tuberculosis. J Comput Assist Tomogr. 2009;33(6):956–60.
15. Chuchottaworn C, Thanachartwet V, Sangsayunh P, Than T, Sahassananda D, Surabotsophon M, et al. Risk Factors for Multidrug-Resistant Tuberculosis among Patients with Pulmonary Tuberculosis at the Central Chest Institute of Thailand. PLoS ONE. 2015;10(10):e0139986.
16. Song Q, Zhang G, Jiang H, Ren Y, Lu X. Imaging Features of Pulmonary CT in Type 2 Diabetic Patients with Multidrug-Resistant Tuberculosis. PLoS ONE. 2016;11(3):e0152507.
17. Lee E, Park C, Goo J, Yim J, Kim H, Lee H, et al. Computed tomography features of extensively drug-resistant pulmonary tuberculosis in non-HIV-infected patients. J Comput Assist Tomogr. 2010;34(4):559–63.
18. Shin H, Choi D, Na J, Choi H, Kim J, Choi H, et al. Low pectoralis muscle index, cavitary nodule or mass and segmental to lobar consolidation as predictors of primary multidrug-resistant tuberculosis: A comparison with primary drug sensitive tuberculosis. PLoS ONE. 2020;15(10):e0239431.
19. Seon H, Kim Y, Lim S, Kim Y, Kwon Y. Clinical significance of residual lesions in chest computed tomography after anti-tuberculosis treatment. Int J Tuberc Lung Dis. 2014;18(3):341–6.
20. Leung A. Pulmonary tuberculosis: the essentials. Radiology. 1999;210(2):307–22.
21. Van Dyck P, Vanhoenacker F, Van den Brande P, De Schepper A. Imaging of pulmonary tuberculosis. Eur Radiol. 2003;13(8):1771–85.
22. Nathella PK, Babu S. Influence of diabetes mellitus on immunity to human tuberculosis. Immunology. 2017;152:13–24.
23. Kumar Nathella P, Babu S. Influence of diabetes mellitus on immunity to human tuberculosis. Immunology. 2017;152(1):13–24.
24. Kumar V, Gu Y, Basu S, Berglund A, Eschrich S, Schabath M, et al. Radiomics: the process and the challenges. Magn Reson Imaging. 2012;30(9):1234–48.
25. Yan Q, Wang W, Zhao W, Zuo L, Wang D, Chai X, et al. Differentiating nontuberculous mycobacterium pulmonary disease from pulmonary tuberculosis

through the analysis of the cavity features in CT images using radiomics. BMC Pulm Med. 2022;22(1):4.
26. Atto A, Berthoumieu Y, Bolon P. 2-D wavelet packet spectrum for texture analysis. IEEE Trans Image Process. 2013;22(6):2495–500.
27. Ha S, Choi H, Cheon GJ, Kang KW, Chung J-K, Kim EE, et al. Autoclustering of Non-small Cell Lung Carcinoma Subtypes on (18)F-FDG PET Using Texture Analysis: A Preliminary Result. Nucl Med Mol Imaging. 2014;48(4):278–86.
28. Gillies R, Kinahan P, Hricak H. Radiomics: Images Are More than Pictures. They Are Data Radiol. 2016;278(2):563–77.

Publisher's note